GEOMAGNETICALLY INDUCED CURRENT SENSITIVITY TO ASSUMED SUBSTATION GROUNDING RESISTANCES IN THE POWER SYSTEM

BY

UYEN BUI

THESIS

Submitted in partial fulfillment of the requirements
for the degree of Master of Science in Electrical and Computer Engineering
in the Graduate College of the
University of Illinois at Urbana-Champaign, 2016

Urbana, Illinois

Adviser:

Professor Thomas J. Overbye

ABSTRACT

A geomagnetic disturbance (GMD) can result in severe damage to the power grid by inducing quasi-dc currents called geomagnetically induced current (GIC). Protection against GMD therefore necessitates the accurate estimation of GIC. GIC estimation is challenging because it depends on substation grounding resistances, which 1) depend more on the local soil and earth conditions than the construction of the substations themselves and 2) can vary by more than an order of magnitude, from 0.05 to 1.5 ohms. Substation grounding resistances are not contained in standard power system models, and approximate values are often used in GIC studies. This motivates the study in this thesis, which proposes a method to calculate the sensitivity of GIC at any substation due to both the substation being studied and neighboring substations' grounding resistances. The work provides an algorithm to quantify the degree of dependence of the GICs at any given substation. The effectiveness of the method is illustrated using parameters from a real-world power system. The case study results using the 20-bus GIC test system and a model of the North American Eastern Interconnect indicate that the substation GICs can be quite dependent on the assumed local substation grounding values. Subsequently, the same systems were studied to include neighboring substation grounding resistances. Although a few cases were dependent on the neighboring values, the local substation grounding resistances were more significant overall. These methods and results are further discussed and analyzed in this work.

This thesis is dedicated to the memory of my dad Duyen Bui, a smart and handsome man whom I still miss every day.

ACKNOWLEDGMENTS

I would like to thank Professor Thomas J. Overbye for his direction in the research and the writing of this thesis. I also want to thank my colleagues in the Power and Energy Systems research group for their technical insight and help.

Lastly, thanks to my husband, my family and friends for their love and support.

TABLE OF CONTENTS

LIST OF TABLES vi

LIST OF FIGURES vii

CHAPTER 1 INTRODUCTION 1

CHAPTER 2 BACKGROUND 3
2.1 Geomagnetic disturbance 3
2.2 Geomagnetically induced current and its negative impacts on the power system 4
2.3 Challenges in measuring time-varying grounding resistances . . 5
2.4 Prior work on the effect of grounding resistances on GIC . . . 10
2.5 Sparse vector/Tinney method 11

CHAPTER 3 MODELING GEOMAGNETICALLY INDUCED CURRENT 17
3.1 Geoelectric field and GMD-induced voltage source 17
3.2 GICs calculation 19

CHAPTER 4 PROPOSED METHODS 23
4.1 Sensitivity to local substation grounding resistance (method 1) 23
4.2 Sensitivity to local and neighboring substation grounding resistance (method 2) 26

CHAPTER 5 CASE STUDIES 31
5.1 EPRI 20-bus 31
5.2 150-bus synthetic system 34

CHAPTER 6 CONCLUSION 38

REFERENCES 39

LIST OF TABLES

2.1 Resistivity of different soil types, adapted from [1] 8

3.1 **G** matrix (in Siemens) for the four bus system 21

5.1 20-bus substation resistances and GIC flows 32
5.2 20-bus substation equivalent values 32
5.3 20-bus system's sensitivity values for a uniform eastward field 33
5.4 20-bus system's sensitivity values for a uniform northward field 33
5.5 150-bus system's 15 substations with the largest GICs and their local sensitivity values for a 3V/km eastward field . . . 36
5.6 150-bus system non-trivial external sensitivity values of 15 substations 37

LIST OF FIGURES

2.1 Solar storm and its effects on the Earth, adapted from [2] . . . 3
2.2 Transformer damage, adapted from [3] 5
2.3 Transformer magnetic flux in normal operation 6
2.4 Saturation of power transformer magnetic flux due to GIC . . 6
2.5 Four-terminal method of measuring earth resistivity, adapted from [1] 7
2.6 Setup of the fall-of-potential method, adapted from [4] 9
2.7 Example factorization graph 14
2.8 Example factorization graph with the forward path {3,7} . . . 14
2.9 Example factorization graph with the backward path {7,6,2} . 15

3.1 GIC flow and voltage source placement, adapted from [5] . . . 19
3.2 A two-substation, four-bus GIC example 20
3.3 Augmented dc network, adapted from [5] 21

5.1 20-bus GIC test system one-line showing 1 V/km eastward values 31
5.2 One-line diagram of 150-bus GMD test case with marks on 15 substations with highest GICs 36

CHAPTER 1

INTRODUCTION

Power systems can suffer heavily from disturbances in the Earth's magnetic field. Changes in the magnetic field induce quasi-DC currents (those with frequency less than 1 Hz) in high voltage, AC transmission lines [6]. As mentioned in [7], this causes half-cycle saturation in the transformers, causing harmonics and increase in reactive power demand. The loss of reactive power support can lead to voltage collapse and/or transformer overheating, potentially resulting in equipment damage.

The effect of such catastrophic disturbances on power systems needs to be understood before preventative measures can be proposed. It is well-known that the geomagnetically induced current (GIC) in a power system can be modeled using elementary current sources [8, 9, 10, 11] as follows. The electric field induced by geomagnetic disturbance (GMD) generates DC currents in the system that can be modeled as DC current sources, denoted by $\mathbf{I}$. Let $\mathbf{G}$ denote the admittance matrix that can be used to find the nodal voltages $\mathbf{V}$ of the system (see Eq. (1.1)).

$$\mathbf{V} = \mathbf{G}^{-1}\mathbf{I} \tag{1.1}$$

Then the GIC at each substation s can be calculated by dividing the corresponding voltage over the substation grounding resistances as shown in Eq. (1.2).

$$I_{\mathrm{GIC},s} = \frac{V_s}{R_s} \tag{1.2}$$

The main contribution of this work is the study of GIC sensitivity with respect to the substation grounding resistance. The rest of the document is organized as follows. Chapter 2 presents the prior work on GIC and the necessary modeling tools needed to study GIC. Chapter 3 presents the GIC model used in this work and Chapter 4 proposes our methods to quantify the sensitivity of GIC with respect to substation grounding resistance, both

for local only and local and neighboring cases. Several case studies illustrate the effectiveness of the proposed approach in Chapter 5. Finally, conclusions are given in Chapter 6.

CHAPTER 2

BACKGROUND

2.1 Geomagnetic disturbance

Geomagnetic disturbance (GMD) is a phenomenon where the Earth's magnetic field changes due to the coronal mass ejection (CME) of the solar wind. The solar wind, or solar flare, is a stream of solar energetic particles (SEPs), i.e. electrons and protons, which is emitted from the corona of the sun to a large distance (see Figure 2.1). Low energy SEPs in solar wind are deflected by the electromagnetic field of the Earth because of not having enough energy. CME is a burst of solar wind and magnetic field and contains high energy SEPs. These SEPs are captured by the Earth's magnetic field, hence disturbing it and creating GMDs. The capturing time is from 20 to 40 hours after the flare occurs and the duration of the change in the magnetic field is about 5 minutes. The solar cycle is 11 years and more severe storms come toward the end of the cycle. The severity of a solar storm is measured in nT/min and classified by Kp-level which ranges from 0 to 9. Any storm

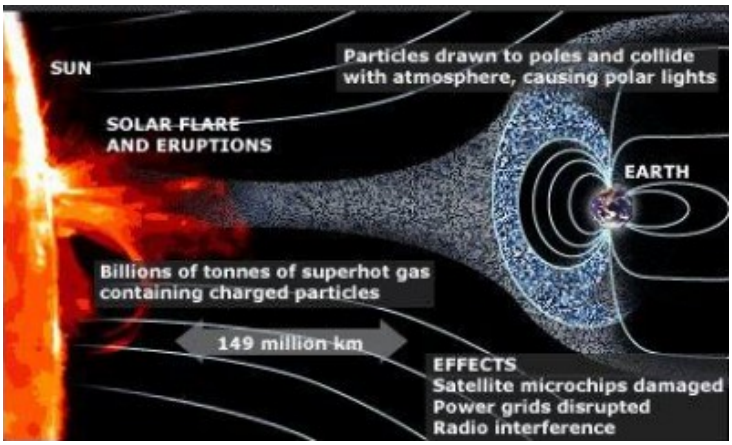

Figure 2.1: Solar storm and its effects on the Earth, adapted from [2]

that is higher than 500 nT/min is considered as Kp level 9 and needs special attention. In one GMD event, the storm polarity and direction can change many times.

2.2 Geomagnetically induced current and its negative impacts on the power system

The change of the Earth's magnetic field creates a geoelectric field at the planet's surface and in the ground, leading to the presence of low frequency (less than 1 Hz) currents in the power system. The current is called geomagnetically induced current (GIC). Because its frequency is very low compared to the system frequency, the current is considered as quasi-DC and is calculated almost like DC current with only conductance values in the electric grid. Since the voltage difference is in the ground and the resistivity of the grounded wire is much lower than that of the soil, the entry point of GICs into the grid is through the grounded neutral wire of wye connected transformers. Similarly, the low resistivity of the high voltage connections compared to the low voltage connections makes them easier for GICs to enter. That is why high voltage transformers are usually the ones with most damage after a GMD event (see Figure 2.2).

The GIC has a significant impact on the operation and stability of many power systems on earth. The most well-known evidence of this impact is the Hydro-Quebec case on March 13, 1989, in which tens of millions of dollars were lost due to a massive blackout that lasted for nine hours [12]. It was reported that the root cause for the collapse of a system with 21,500 MW generation and 2,000 kilometers of power lines was due to the tripping of 7 static VAR compensators (SVCs) in 59 seconds, leading to 9,460 MW output lost from Hydro-Quebec's La Grande Hydroelectric Complex. The balance between the loads connected to the power grid was restored by the load-reduction system's disconnected regions in Quebec. Twenty-five seconds later the entire Quebec power grid collapsed.

GIC can cause voltage instability, and consequently system collapse, through the loss of reactive power in power systems. The DC flux created by GIC in the core power transformer shifts its operating point on the magnetizing curve. The shift causes flux saturation in half of the 60 Hz cycle, creating a

Figure 2.2: Transformer damage, adapted from [3]

burst in the magnetizing current magnitude (compare Figures 2.3 and 2.4), which is referred as the half-cycle saturation phenomenon in the transformer. During this saturation, the transformer consumes a significant amount of reactive power of the system, leading to reactive power loss in the network. In severe cases it can lead to system failure because of the voltage collapse. In addition, the half-cycle saturation introduces harmonics to the power line currents, which results in increase in the eddy-current loss and core loss in transformers and generators. These losses subsequently cause heating and severe damage in those components. Because of the sensitivity of electromechanical relays to current harmonics, the harmonics also cause the power protections to improperly operate, which leads to the tripping of capacitor banks and static VAR compensations (SVCs). This results in the significant loss of reactive power support when the system is in need of it the most and drives the system closer to a collapse.

2.3 Challenges in measuring time-varying grounding resistances

Substation grounding resistance represents the interconnected impedance of the grounding system of a substation. The impedance is usually measured in terms of resistance because the reactance is generally negligible with respect to the resistive component. The reactive component is only needed when the

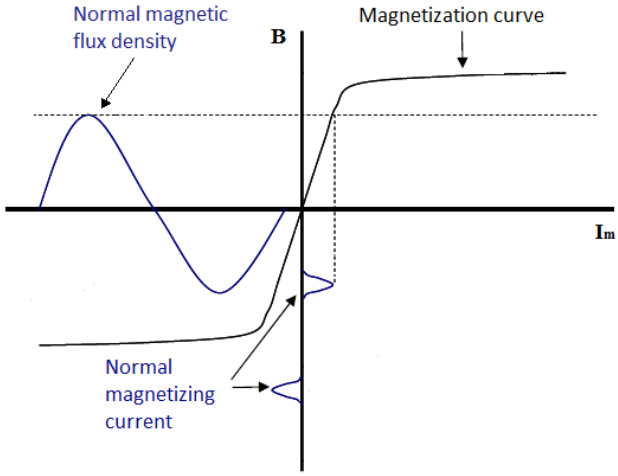

Figure 2.3: Transformer magnetic flux in normal operation

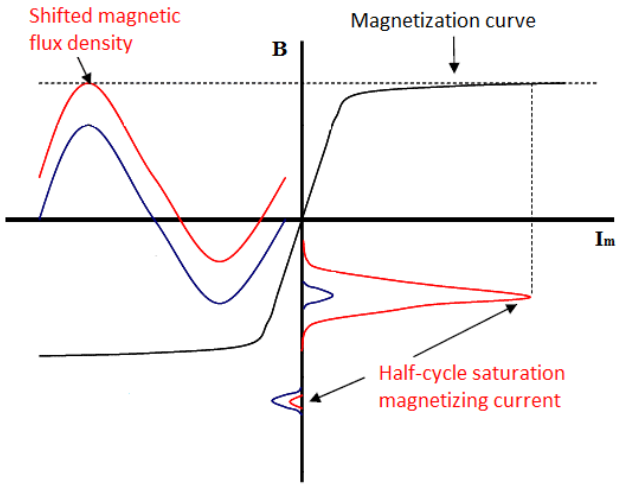

Figure 2.4: Saturation of power transformer magnetic flux due to GIC

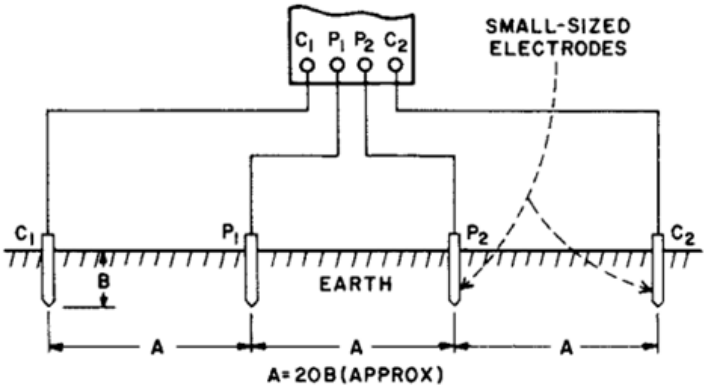

Figure 2.5: Four-terminal method of measuring earth resistivity, adapted from [1]

analysis involves surge or impulse currents. The grounding resistance consists of the grounding mat that covers a large area of many buried grounding electrodes and the ground paths emanating out from the substation such as those due to shield wire grounding. It primarily depends on the resistivity of the soil and the size and construction of the ground grid [4].

Earth resistivity, measured in Ω-cm, is the resistance of the soil with respect to an electrode system. A common method to measure the earth resistivity is called the four-terminal method, which is illustrated in Figure 2.5. In this figure, four small electrodes are driven down to the same depth (B) and equal distances (A) apart in a straight line, and four separate lead wires connect the electrodes to the four terminals on the instrument.

As shown by Dr. Frank Wenner of the U.S. Bureau of Standards in 1915, for B sufficiently smaller than A, i.e. 20 times, the following formula can be applied:

$$\rho = 2\pi AR \tag{2.1}$$

In the equation, ρ is the average soil resistivity to depth A in Ω-cm, A is the distance between the electrodes in cm, and R is the earth resistivity tester reading in ohms. In the example, if the distance between the electrodes is 4 ft and the reading on the tester is 20 Ω, the average earth resistivity to a depth of 4 ft is calculated as

$$\rho = 2 \times 3.1416 \times (4 \times 30.48) \times 20 = 15,320 \text{ Ω-cm} \tag{2.2}$$

Table 2.1: Resistivity of different soil types, adapted from [1]

Soil	Resistivity (Ω-cm)		
	Avg	Min	Max
Fills: ashes, cinders, brine wastes	2,370	590	7,000
Clay: shale, gumbo, loam	4,060	340	16,300
Varying proportions of sand/gravel	15,800	1,020	135,000
Gravel, sand, stones with little clay/loam	94,000	59,000	458,000

The centimeter unit can be converted to meters or miles when needed. The result above is equal to 153.2 Ω-m and is about the resistivity of topsoil.

The type of soil affects the value of the earth resistivity tremendously whether it is largely clay or very sandy. Table 2.1 shows average, min, and max values for different types of soil. At a given location, the soil can be composed of various combinations of dry soil, clay, gravel, slate, and sandstone. It can be moderately homogeneous over a large area, or it can be layered in granite, sand, or other high-resistivity materials. Hence we cannot say that a given soil has a resistivity of so many Ω-cm, but must measure it.

The soil resistivity decreases with moisture and dissolved salts because of the electrolytic characteristic of the current. The amount of water in the soil and its salt content vary with the weather, time of year, and the nature of the subsoil. In fact, pure water has nearly infinitely high resistivity and the dissolved naturally occurring salts in the earth lower the resistivity. Only a small amount of salt can significantly change the soil resistivity. In addition, the increase of temperature also decreases the resistivity of the soil. From the effects of the moisture, the salt content, and the temperature, it is clear that the earth resistivity will vary considerably over the course of a year. Therefore, the grounding resistance will also vary with time.

Devices are physically grounded by having a conductor in physical contact with the ground. Grounding resistance can be calculated with the knowledge of the earth resistivity and the conductor/electrode parameters. To determine the resistance R of the ground, we can treat it with Ohm's law like any other resistive material as:

$$R = \frac{\rho \times \text{conductor length}}{\text{cross sectional area}} \tag{2.3}$$

The average resistivity of good conductors like aluminum and copper is

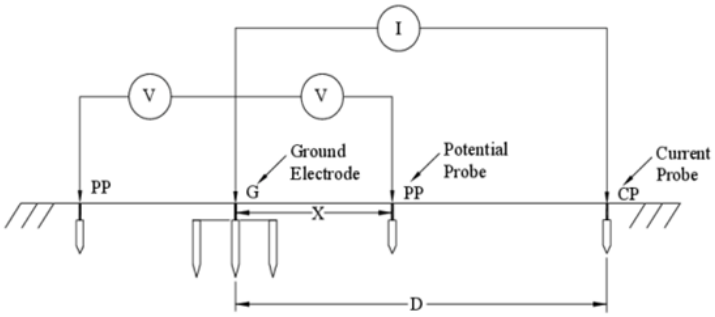

Figure 2.6: Setup of the fall-of-potential method, adapted from [4]

about $2 \times 10 - 8$ Ω-m while the average resistivity of topsoil is 160 Ω-m and sand/gravel is 900 Ω-m. However, because of its vast cross sectional area, the earth is actually a good conductor. A circular wire made of topsoil with radius of 500 m, 1 mile long, has a resistance of about 0.3 Ω.

In reality, the grounding resistance is not calculated based on the resistivity of the soil and the structure of the ground grid, but measured using meters and testers. Two main reasons are the inadequacy of the analytical methods used in the calculations of the resistance and the possibility of a change in the soil resistivity. Many methods have been used to obtain this resistance: two-point method, three-point method, fall-of-potential method (see Figure 2.6), ratio method, slope method, staged fault tests, and resistance measurements by clamp-on method. The fall-of-potential is more commonly used and can provide an accurate result if properly conducted. The method involves passing a current between a ground electrode (G) and a current probe (CP), and then measuring the voltage between G and a potential probe (PP).

The current probe is generally placed at a substantial distance from the ground electrode under test to minimize interelectrode influences due to mutual resistances. This distance should be at least five times the largest dimension of the ground electrode under test. In addition, the location of the potential probe plays an important role in measuring the resistance of the ground electrode since it needs to be free from any influence by both the ground electrode and the current probe. In practice, the distance for the potential probe is often chosen to be 65% of the distance to the current probe, provided that they are in the same direction. This 65% rule is based on a theoretical calculation by Curdts in [13]. The main advantage of the fall-of-potential method is that it produces an accurate measurement even when the

potential and current electrodes have a substantially higher resistance than the ground being tested.

Although the fall-of-potential method gives highly reliable results, it also comes with some inevitable problems. First, it is extremely time-consuming and labor intensive; the nature of substation and power station grounding systems makes the testing far more complicated than on a simple ground electrode. Secondly, the large area of a substation and power station ground system results in a large resistance area and therefore long distances to the test probes. The current test probe should be placed 10 times the maximum distance on the ground system to find the flat portion of the characteristic resistance curve. Third, the typical grounding resistance is from 0.1 Ω to 1 Ω, and if the test instrument resolution is not sufficiently small then it will lead to reading error. To solve this problem, the instrument used should have 1 mΩ measurement resolution. Also it has to be specifically designed to overcome the noise from power utility and switching. Last but not least, individual ground electrodes must be disconnected from the system to be measured, and, in reality, there are situations where disconnection is not possible. These problems make the measuring procedure for substation grounding resistance too difficult to conduct regularly.

Because of the variation with time of year and the difficulty in obtaining updated measuring values, the substation grounding resistance, a key piece of information needed to construct G and so to obtain the GIC values in the system, is usually not accurately available. That is why a method to indicate which grounding resistance concrete values are most needed is helpful in predicting the GICs that will occur in the system under an incoming GMD event.

2.4 Prior work on the effect of grounding resistances on GIC

Pirjola [14] is among the earliest authors to investigate the effect of grounding resistance on GIC. Through a series of case-study computations, Pirjola showed that, for sufficiently small uncertainties in the grounding resistance, their impacts are insignificant in practical applications (where only the level of GIC, rather than its precise values, is needed). In addition, it was also

shown that the interactions between different stations, i.e. the effects of off-diagonal elements in the earthing impedance matrix, are modest. However, these conclusions are based on macro-adjustments to all grounding resistances simultaneously. In contrast, our research takes a different approach where only one (either local or neighboring) grounding resistance is adjusted at a time. Namely, the sensitivity of the GIC with respect to a grounding resistance is explicitly quantified. With this approach, it is discovered that the change in a GIC with respect to a grounding resistance is nontrivial.

The proposed method is presented in Chapter 4. The method itself relies heavily on the celebrated sparse vector/Tinney technique, which is briefly reviewed in the Section 2.5.

2.5 Sparse vector/Tinney method

Sparse vector method, originally proposed by Tinney et al. [15], is an efficient algorithm for solving sparse linear inverse problems. The general form of a linear inverse problem is given as follows:

$$Ax = b \tag{2.4}$$

where A is a nonsingular (square) matrix of dimension N, b is the vector of measurements, and x is the unknown. Since A is nonsingular, x is given by

$$x = A^{-1}b \tag{2.5}$$

The matrix A can be further decomposed into a product of matrices with special structures. Namely,

$$A = LDU \tag{2.6}$$

where L, U are unit triangular matrices whose elements above/below the diagonal are all zeros, respectively, and D is a diagonal matrix. The special structures of L, D, U simplify the procedure in (2.5) into simple operations of forward and backward substitutions. Namely,

$$\begin{aligned} w &= D^{-1}L^{-1}b \qquad \text{(forward substitution)} \\ x &= U^{-1}w \qquad \text{(backward substitution)} \end{aligned} \tag{2.7}$$

The following example is used to illustrate Eq. (2.7). Let

$$A = \begin{bmatrix} 1 & 0 & 0 & 2 & 2 & 0 & 0 \\ 0 & 1 & 0 & 0 & 0 & 0.5 & 1 \\ 0 & 0 & 1 & 0 & 0 & 0 & 2 \\ 2 & 0 & 0 & 5 & 6 & 0 & 0 \\ 2 & 0 & 0 & 6 & 9 & 3 & 0 \\ 0 & 0.5 & 0 & 0 & 3 & 10.25 & 5.5 \\ 0 & 1 & 2 & 0 & 0 & 5.5 & 31 \end{bmatrix}, b = \begin{bmatrix} 0 \\ 0 \\ 2 \\ 0 \\ 0 \\ 0 \\ 0 \end{bmatrix} \tag{2.8}$$

Then with LDU composition,

$$\begin{aligned} L &= \begin{bmatrix} 1 & 0 & 0 & 0 & 0 & 0 & 0 \\ 0 & 1 & 0 & 0 & 0 & 0 & 0 \\ 0 & 0 & 1 & 0 & 0 & 0 & 0 \\ 2 & 0 & 0 & 1 & 0 & 0 & 0 \\ 2 & 0 & 0 & 2 & 1 & 0 & 0 \\ 0 & 0.5 & 0 & 0 & 3 & 1 & 0 \\ 0 & 1 & 2 & 0 & 0 & 5 & 1 \end{bmatrix} \\ U &= L^T \\ D &= I \end{aligned} \tag{2.9}$$

The auxiliary vector w can therefore be obtained using elementary operations as follows:

$$w = \begin{bmatrix} b_1 \\ b_2 \\ b_3 \\ b_4 - 2w_1 \\ b_5 - 2w_1 - 2w_4 \\ b_6 - 0.5w_2 - 3w_5 \\ b_7 - w_2 - 2w_3 - 5w_6 \end{bmatrix} = \begin{bmatrix} 0 \\ 0 \\ 2 \\ 0 \\ 0 \\ 0 \\ -4 \end{bmatrix} \tag{2.10}$$

where the subscripts are used to index elements in a vector. Notice that each element of w is only a function of elements with lower indices, hence the name forward substitution. From w, the solution x can be obtained using

(backward) substitutions as follows:

$$x = \begin{bmatrix} w_1 - 2x_4 - 2x_5 \\ w_2 - 0.5x_6 - x_7 \\ w_3 - 2x_7 \\ w_4 - 2x_5 \\ w_5 - 3x_6 \\ w_6 - 5x_7 \\ w_7 \end{bmatrix} = \begin{bmatrix} -120 \\ -6 \\ 10 \\ 120 \\ -60 \\ 20 \\ -4 \end{bmatrix} \tag{2.11}$$

Again, notice that each element of x is only a function of elements with higher indices, hence the name backward substitution.

The above forward/backward substitution algorithm is computationally intensive, i.e. $O(N^3)$. Fortunately, a more efficient algorithm, first discovered by Tinney et al. [15], exists. The algorithm works by exploiting the fact that there are very few non-zero elements in both A and b in Eq. (2.8), and if only a subset of the unknown vector x is desirable, i.e. the linear inverse problem is *sparse*, then the algorithm relies on the core concept of a factorization graph.

A factorization graph is a graph whose nodes represent column/row indices of the matrix A. The connections between nodes form a factorization path that defines an ordered list of columns/rows on which forward/backward substitutions shall be executed. The motivation behind the construction of a factorization graph is the observation that, for sparse linear inverse problems, only a few forward/backward operations are needed to produce the result. Hence, Tinney's algorithm reduces the computational complexity by executing only those non-trivial operations, i.e. fast forward (FF) and backward (FB), which are identified by factorization paths.

To illustrate the usefulness of a factorization graph, it is assumed that one is given (see Figure 2.7) for the inverse problem in Eq. (2.8). b_3 is the only non-zero element in b so according to Figure 2.8, FF substitution consists of

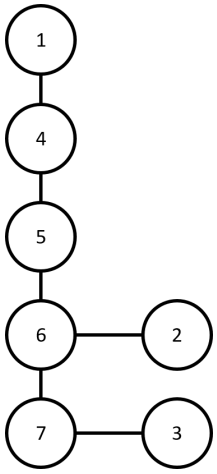

Figure 2.7: Example factorization graph

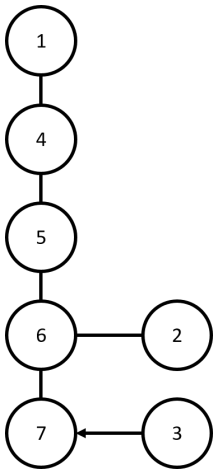

Figure 2.8: Example factorization graph with the forward path {3,7}

only operations at indices 3 and 7; therefore, it follows that

$$L \begin{bmatrix} 0 \\ 0 \\ w_3 \\ 0 \\ 0 \\ 0 \\ w_7 \end{bmatrix} = \begin{bmatrix} 0 \\ 0 \\ 2 \\ 0 \\ 0 \\ 0 \\ 0 \end{bmatrix} \Leftrightarrow \begin{cases} w_3 & = 2 \\ w_7 & = -2w_3 = -4 \end{cases} \tag{2.12}$$

Now if x_2 is desirable, then FB substitution consists of only operations at

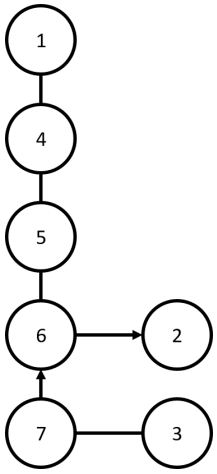

Figure 2.9: Example factorization graph with the backward path {7,6,2}

indices 7, 6, and 2 (see Figure 2.9). Namely,

$$U \begin{bmatrix} \\ x_2 \\ \\ \\ \\ x_6 \\ x_7 \end{bmatrix} = \begin{bmatrix} 0 \\ 0 \\ 2 \\ 0 \\ 0 \\ 0 \\ -4 \end{bmatrix} \Leftrightarrow \begin{cases} x_7 & = w_7 = -4 \\ x_6 & = -5x_7 = 20 \\ x_2 & = -0.5x_6 - x_7 = -6 \end{cases} \tag{2.13}$$

Similarly, if x_5 is desirable, then the backward path {7,6,5} can be used.

$$U \begin{bmatrix} \\ \\ \\ \\ x_5 \\ x_6 \\ x_7 \end{bmatrix} = \begin{bmatrix} 0 \\ 0 \\ 2 \\ 0 \\ 0 \\ 0 \\ -4 \end{bmatrix} \Leftrightarrow \begin{cases} x_7 & = w_7 = -4 \\ x_6 & = -5x_7 = 20 \\ x_5 & = -3x_6 = -60 \end{cases} \tag{2.14}$$

The construction of the factorization graph in Figure 2.7 is discussed next. Consider the L matrix in Eq. (2.6). For the column 1, since the lowest index of a non-zero element below the diagonal is 4, Tinney's algorithm dictates that node 1 connects to node 4. Next, the algorithm proceeds to column 4 and finds that the lowest index of a non-zero element below the diagonal is 5.

Hence the algorithm dictates that node 4 connects to node 5. Similarly, node 5 connects to node 6, and node 6 connects to node 7. Now the nodes that have not yet been considered are 2 and 3. Repeating the above procedure for column 2 reveals that node 2 connects to node 6. Similarly, analyzing column 3 shows that node 3 connects to node 7. Once all nodes are considered, the factorization graph in Figure 2.7 is complete.

The improvement of the FF and FB method proposed by Tinney et al. over the standard forward and backward substitutions depends on the sparsity structure of the matrix A, the measurement vector b, and the requirement on the unknown vector x. In particular, the improvement of FF depends on the sparsity structure of L and b, while the improvement of FB depends on the sparsity structure of U and x, i.e. the number of elements in x that is desirable. To precisely measure the improvement of Tinney's sparse vector method, one can use the ratio of the number of multiply-and-add operations used in FF and FB to that of the standard forward and backward procedure, i.e.

$$R = \frac{\text{mult-adds in FF and FB}}{\text{mult-adds in standard forward and backward}} \tag{2.15}$$

CHAPTER 3

MODELING GEOMAGNETICALLY INDUCED CURRENT

3.1 Geoelectric field and GMD-induced voltage source

Many methods have been proposed to model the impact of solar storms on the power system, two of which are presented in [16] and [17]. The ultimate goal of the modeling is to give an accurate mapping from the storm profile to geoelectric fields to use in calculation of GICs. A non-uniform geomagnetic storm profile is characterized by the rate of change of the magnetic field density vector $\mathbf{B}$ in units of nT/min, which data is recorded from magnetometer stations. The interaction between the storm and the Earth's magnetic field can be approximated by Faraday's law.

$$\int \frac{\partial \mathbf{B}}{\partial t} \mathrm{d}\mathbf{A} = \frac{\partial \mathbf{\Phi}_B}{\partial t} = \epsilon \tag{3.1}$$

The geoelectric field is calculated as an integral of the rate of change of the magnetic field density $\mathbf{B}$ over an area $\mathbf{A}$. The field also depends on the Earth's varying ground conductivity, so the conductivity model is an important part in obtaining the electric field. Fortunately, for basic study of power systems in GMD events, a uniform geoelectric field for which the conductivity model is not needed is good enough because GMDs are continental in scope. On the other hand, for a big power grid spread over a large geographic area, it is critical to know the ground conductivity in order to map the magnetic disturbance to the geoelectric field. The modeling result is judged based on historical data of GMD events.

The effect of the geoelectric field on the power system is represented as voltage sources in the system. A voltage source is the voltage difference between geographical locations due to the induced electric field and is calculated as:

$$V_{\mathrm{dc}} = \oint \mathbf{E} \cdot \mathrm{d}\mathbf{l} \tag{3.2}$$

where V_{dc} is the voltage source, $\mathbf{E}$ is the electric field vector, and $\mathbf{l}$ is the vector of the path. There are two methods to integrate this voltage in the system: either as DC voltage source in the ground or as DC voltage source in series with the transmission lines. However, only the transmission line approach works for the realistic non-uniform geoelectric field. The reason is that only a uniform electric field is "conservative", meaning its integration along any path depends not on the path itself but on the distance between the start and the end points. Hence, the integral around a closed loop is zero. However, this rule does not apply to non-uniform fields, so modeling the voltage source in the ground is not valid in general cases.

The dot product in Eq. (3.2) shows that the voltage depends greatly on the direction of the electric field vector with respect to the transmission line. If they are perpendicular to each other, then there is no voltage induced on the line at all. This means that power systems can be vulnerable to geoelectric fields with particular orientations and identifying them can be important in protecting the systems.

As mentioned above, a uniform field is a good starting point for studying power systems under GMD events. With the assumption that the geolectric field is constant over the length of the transmission line, the dc voltage source on the line can be calculated as:

$$V = E_N L_N + E_E L_E \tag{3.3}$$

In the case of non-uniform field, by diving the line into small segments and applying the uniform assumption on each of them, the voltage source is approximated as the sum of the induced voltages on those segments.

The induced voltage sources then are represented as Norton equivalent current injections into buses. In example, the DC voltage source in series with line (a,b) V_{ab} (with the positive polarity on the a side) is converted to a Norton equivalent DC current source on the line as

$$I_{ab} = V_{ab}/R_{ab} \tag{3.4}$$

where R_{ab} is the series resistance of the transmission line (a,b). From Kir-

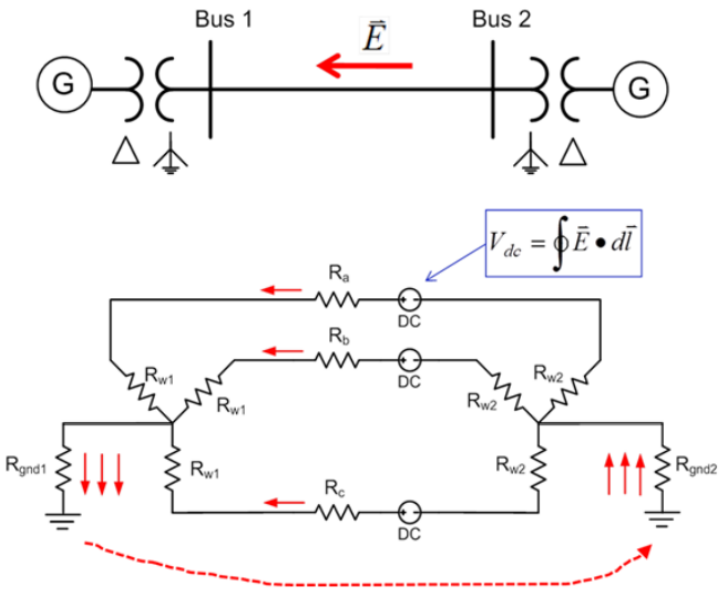

Figure 3.1: GIC flow and voltage source placement, adapted from [5]

choff's law, the overall current injection to bus a is calculated as the sum of all Norton equivalent DC currents entering or leaving bus a through all transmission lines connected to it.

3.2 GICs calculation

Figure 3.1 demonstrates how GICs flow in the system; they enter and exit through the grounded neutral of the wye connected transformer. With the knowledge of the network topology and parameters, induced transmission line voltage sources, transformers parameters and power systems substation grounding resistance, the GICs in the system can be calculated by solving the equation:

$$\mathbf{V} = \mathbf{G}^{-1}\mathbf{I} \tag{3.5}$$

where vector $\mathbf{I}$ is the vector of all Norton equivalent DC current injections which are derived in Section 3.1. $\mathbf{G}$ is a matrix with structure similar to that of the power system bus admittance matrix except 1) it is a real matrix with just conductance values, 2) conductance values are determined by the parallel combination of the three individual phase resistances, 3) $\mathbf{G}$ is

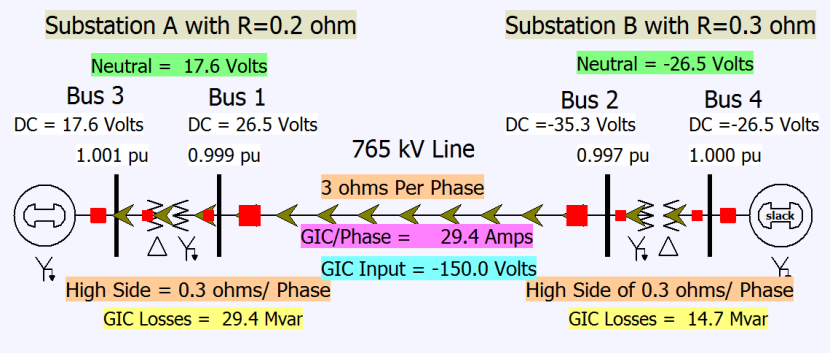

Figure 3.2: A two-substation, four-bus GIC example

augmented to include the substation neutral buses and substation grounding resistance values, 4) transmission lines with series capacitive compensation are omitted since series capacitors block DC flow, and 5) transformers are modeled with their winding resistance to the substation neutral in the case of autotransformers.

When solved, the voltage vector $\mathbf{V}$ contains entries for the s substation neutral DC voltages and the m bus DC voltages. Throughout this thesis it is assumed that the s substations are ordered as the first entries in $\mathbf{V}$, and the m buses are ordered as the $s+1$ to $s+m$ entries. The $\mathbf{V}$ vector can be used to calculate all the GICs in the system. The GIC flow at a substation A can be obtained by Ohm's law, as given by

$$I_{\text{GIC},A} = V_A / R_A \tag{3.6}$$

where R_A is the substation grounding resistance of substation A. Note that this GIC is not the same as the DC current injection in the previous section.

For demonstration, consider the simple network in Figure 3.2 with two generators and four buses: Bus 1 and its generator (Bus 3) in Substation A, and Bus 2 with its generator (Bus 4) in Substation B. The high voltage generator step-up transformers are grounded wye on their high sides. Buses 1 and 2 are connected by a 765 kV line that has a per phase resistance of 3 Ω; the per phase resistance of the high side coil of each of the two transformers is 0.3 Ω, a grounding resistance of 0.2 Ω for Substation A and 0.3 Ω for Substation B. Assume the substations are at the same latitude, separated by 150 km in the east-west direction, with a given electric field of 1 V/km in the east-west direction. This gives an induced voltage in the transmission line of

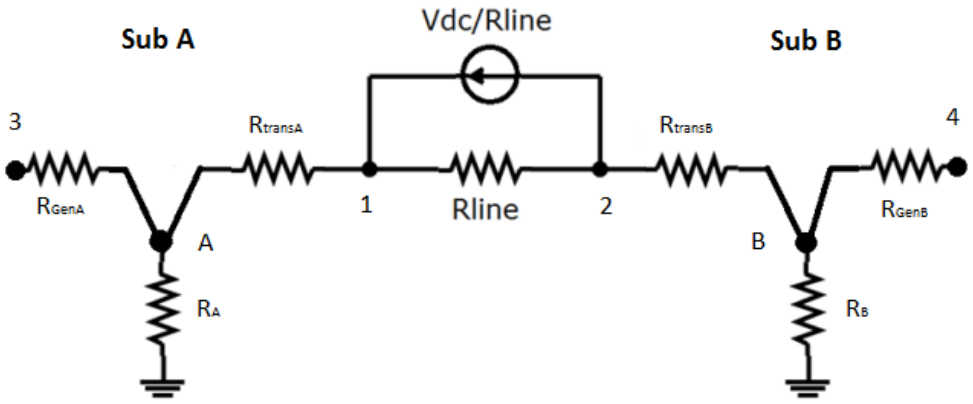

Figure 3.3: Augmented dc network, adapted from [5]

Table 3.1: **G** matrix (in Siemens) for the four bus system

	Sub A	Sub B	Sub C	Sub D
Sub A	15.00	0.00	-10.00	0.00
Sub B	0.00	13.33	0.00	-10.00
Bus 1	-10.00	0.00	11.00	-1.00
Bus 2	0.00	-10.00	-1.00	11.00

150 V.

The GICs in the system are calculated by solving Eq. (3.5) and then Eq. (3.6). For the construction of the **G** matrix in Table 3.1, the system is augmented as in Figure 3.3 to include substation neutral buses (buses A and B). Since the low-side generator buses (Buses 3 and 4) are delta-connected, they have no any impact on the GICs and are omitted in the equation. This rule is applied to all low-side generator buses in bigger and more complex networks like those in Chapter 5. By discarding them, the values of the generator resistances are no longer needed.

$$\begin{bmatrix} 15 & 0 & -10 & 0 \\ 0 & 13.33 & 0 & -10 \\ -10 & 0 & 11 & -1 \\ 0 & -10 & -1 & 11 \end{bmatrix} \begin{bmatrix} V_A \\ V_B \\ V_1 \\ V_2 \end{bmatrix} = \begin{bmatrix} 0 \\ 0 \\ V_{\mathrm{dc}}/R_{\mathrm{line}} \\ -V_{\mathrm{dc}}/R_{\mathrm{line}} \end{bmatrix} \tag{3.7}$$

$$\mathbf{V} = \begin{bmatrix} V_A \\ V_B \\ V_1 \\ V_2 \end{bmatrix} = \begin{bmatrix} 17.6 \\ -26.5 \\ 26.5 \\ -35.3 \end{bmatrix} V \tag{3.8}$$

From the values of the dc voltage at substation neutral bus A, the GIC flow through Substation A to the ground can be calculated as follows:

$$I_{\text{GIC},A} = \frac{V_A}{R_A} = \frac{17.6V}{0.2\Omega} = 88A \tag{3.9}$$

Similarly, Substation Bs GIC can be obtained with the values of V_B and R_B and equal to -88 A. It can be explained that an 88 A quasi-dc current results from the GMD flows from the ground through Substation B grounding resistance into the high side coil of the Substation B transformer, down the 765 kV line into the high voltage coil in Substation A and back into the ground through Substation A grounding resistance. In Figure 3.2 which comes from PowerWorld simulation, the direction and size of the arrows are used to visualize the direction and magnitude of the GIC flow.

CHAPTER 4

PROPOSED METHODS

4.1 Sensitivity to local substation grounding resistance (method 1)

Method 1 is employed at the beginning of this study about GIC sensitivity to substation grounding resistance because it is simple and straightforward. However, it only works for the grounding resistance of the substation whose GIC is being studied; that leads to the creation of method 2, which can solve for the sensitivities to resistances of both local and neighboring substations. Regardless, the first method still gives a good idea about how the uncertainty of the values of grounding resistances can affect the reliability of the calculated values of GICs.

We use the same example in Section 3.2, but this time directly calculate the GICs by solving a simple DC circuit. From a GIC perspective, the three phases of the transmission line and transformers are in parallel, so the total three-phase resistance for the 765 kV line is $(3/3)\ \Omega = 1\ \Omega$, and $(0.3/3)\ \Omega = 0.1\ \Omega$ for each of the transformers. These resistance values are then in series with the Substation A and B grounding resistance, which leads to

$$I_{\mathrm{GIC}} = \frac{150\ \mathrm{V}}{(1 + 0.1 + 0.1 + 0.2 + 0.3)\ \Omega} = 88.26\ \mathrm{A} \tag{4.1}$$

The 88.26 A result gives the total current in all three phases (i.e., 29.4 A per phase). Using Eq. (4.1), it is possible to obtain the sensitivity of I_{GIC} to each of the model parameters. Focusing on the sensitivity of I_{GIC} with respect to the Substation A grounding resistance, R_A, Eq. (4.1) can be rewritten as

$$I_{\mathrm{GIC},A} = \frac{150V}{(1 + 0.1 + 0.1 + 0.3 + R_A)\Omega} = \frac{V_{\mathrm{TH},A}}{R_A + R_{\mathrm{TH},A}} \tag{4.2}$$

where $V_{\mathrm{TH},A}$ is the Thevenin equivalent voltage looking into the network from Substation A, and $R_{\mathrm{TH},A}$ is the corresponding Thevenin equivalent resistance. For this example, their values are 150 V and 1.5 Ω respectively; $I_{\mathrm{GIC},A}$ is the current flowing into the ground through the Substation A resistance. The sensitivity of $I_{\mathrm{GIC},A}$ to the variation in the assumed value for R_A is calculated by differentiating Eq. (4.2) with respect to R_A,

$$\frac{\partial I_{\mathrm{GIC},A}}{\partial R_A} = \frac{-V_{\mathrm{TH},A}}{(R_A + R_{\mathrm{TH},A})^2} \tag{4.3}$$

which shows that $I_{\mathrm{GIC},A}$ can be changed equally by a variation in either R_A or in $R_{\mathrm{TH},A}$.

However, these quantities are often known with potentially vastly different degrees of accuracy. The substation grounding resistance is often an approximation with a high degree of uncertainty. In contrast, $R_{\mathrm{TH},A}$ is mostly based on values known with a relatively high degree of precision, including the transmission line and transformer resistances. While [18] makes the important observation that wire resistance is temperature dependent, this variation of about 0.4% per degree C is known and therefore can be included in a study by using an approximate temperature profile. Also, it is apparent in this simple example that $R_{\mathrm{TH},A}$ depends upon the assumed resistance of the other substation.

Using Eq. (4.3) we can obtain the sensitivity of the substation GIC to variation in assumed substation resistance in terms of a normalized variation, that is, the percent variation in the current in terms of the percent variation in the grounding resistance. For the general case of an arbitrary substation i, this can be expressed as

$$\frac{\partial(\%I_{\mathrm{GIC},i})}{\partial(\%R_i)} = \frac{\frac{\partial I_{\mathrm{GIC},i}}{I_{\mathrm{GIC},i}}}{\frac{\partial R_i}{R_i}} = \frac{-R_i}{R_i + R_{\mathrm{TH},i}} \tag{4.4}$$

Note that this sensitivity is always negative since an increase in assumed resistance will always result in a decrease in the magnitude of the current. Hence, it is convenient to define the absolute of this ratio as

$$\Re_i = \frac{R_i}{R_i + R_{\mathrm{TH},i}} \tag{4.5}$$

If the $\Re_i$ is small (i.e. the Thevenin resistance is substantially larger than

the substation resistance), as in this example, then an accurate estimate of substation resistance is less important. Conversely, if $\Re_i$ approaches unity then the value of the substation resistance dominates in the determination of $I_{\text{GIC},i}$.

Returning to the four-bus example,

$$\Re_A = \frac{0.2}{0.2 + 1.5} = 0.1176 \tag{4.6}$$

which indicates that a 1.0% error in R_i results in a 0.1176% error in $I_{\text{GIC},A}$. So if the assumed value of R_A is increased by say 10% (from 0.2 to 0.22 Ω) the magnitude of $I_{\text{GIC},A}$ decreases by about (0.1176)*(10%) = 1.176%. Of course, this is only a linearization about the current estimate of R_i. For example, if the value of R_A were assumed to increase by 100% (changing to 0.4 Ω) the value of $I_{\text{GIC},A}$ would only decrease by about 10.6% (to 78.9 A).

Since the Thevenin equivalence resistance can be obtained for any substation in a network by calculating the diagonal element of $\mathbf{G}^{-1}$ corresponding to the substation, this approach can be generalized to systems of any size. Define the resistance matrix as

$$\mathbf{R} = \mathbf{G}^{-1} \tag{4.7}$$

Then, with the assumption that the s substations are ordered as the first s entries in $\mathbf{G}$, the driving point resistance for the i-th substation is $\mathbf{R}_{ii}$. Since for large systems $\mathbf{G}$ is quite sparse, the diagonal elements of $\mathbf{R}$ can be calculated with great computational efficiently using sparse vector methods (see Section 2.5). It is important to emphasize that the entire matrix $\mathbf{G}$ is never explicitly inverted.

Since the substation resistances are directly connected to ground, the driving point resistance is the parallel combination of substation resistance and the Thevenin resistance, given by

$$\mathbf{R}_{ii} = \frac{1}{\frac{1}{R_i} + \frac{1}{R_{\text{TH},i}}} \tag{4.8}$$

where R_i is the grounding resistance of the i-th substation, and $R_{\text{TH},i}$ is the Thevenin resistance looking into the network from the same substation. Solving (4.8) for $R_{\text{TH},i}$ gives

$$R_{\mathrm{TH},i} = \frac{1}{\frac{1}{\mathbf{R}_{ii}} - \frac{1}{R_i}} \tag{4.9}$$

Before demonstrating the matrix approach on the four-bus system and moving on to larger systems, several observations are warranted. First, the Thevenin voltages are dependent upon the $\mathbf{I}$ vector used in (3.5), which means they do depend upon the particular GMD scenario under consideration. Second and conversely, the Thevenin resistance values are independent of $\mathbf{I}$, depending only upon $\mathbf{G}$. Third, the substations for which accurate resistance values are most needed are those that have both high GIC values and high ratio values ($\Re$).

4.2 Sensitivity to local and neighboring substation grounding resistance (method 2)

Compared to method 1, method 2 is more complicated, but is capable of computing the sensitivity of GIC to the grounding resistance of the substation being studied and, most importantly, to the grounding resistance of other substations in the network which is not possible using method 1. Equation (4.2) of the two-substation, four-bus system example shows that GIC depends not only on R_A but also on $R_{\mathrm{TH},A}$, which is the Thevenin resistance from Substation A looking back into the system. Its value is mainly composed of the resistances of the system's transmission lines and transformers. However, it is apparent that $R_{\mathrm{TH},A}$ also depends upon the assumed grounding resistance of the other substations; as in the example, it includes R_B which is the grounding resistance of Substation B. Hence, the effect of variation in the assumed grounding resistances of neighboring substations cannot be neglected in this study of GIC sensitivity.

This section addresses the issue of sensitivity to grounding resistances by proposing an algorithm to calculate the sensitivity of GIC on any substation with respect to both local and other substations' grounding resistances. With this function, utility companies can identify the worst-case scenario without updated and accurate grounding resistance values and can better prepare for potential GMD events.

4.2.1 Sensitivity of GICs to local resistance

Consider a general system that has s substations and m buses. The variation of the approximated grounding resistance R_i is interpreted as the variation of the corresponding conductance g_i, notated as $\tilde{g}_i$.

$$\tilde{g}_i = g_i' - g_i \tag{4.10}$$

where g_i is the assumed grounding conductance of substation i, g_i is the new g_i, and $\tilde{g}_i$ denotes the change or variation. This change leads to the change in the matrix $\mathbf{G}$ and is denoted as $\mathbf{G}'$

$$\mathbf{G}' = \mathbf{G} + g_i e_i e_i^T \tag{4.11}$$

where e_i is a $n \times 1$ vector with the element in the i-th row being 1 and 0 otherwise; e_i^T is the transpose of e_i. Using matrix inversion lemma, the inverse of matrix $\mathbf{G}'$ is given as

$$\mathbf{G}'^{-1} = \mathbf{G}^{-1} - \mathbf{G}^{-1} e_i (\tilde{g}_i^{-1} + e_i^T \mathbf{G}^{-1} e_i)^{-1} e_i^T \mathbf{G}^{-1} \tag{4.12}$$

Then, the GIC at substation i can be written in terms of conductance g_i, matrix $\mathbf{G}$, and the current injection vector $\mathbf{I}$.

$$I_{\mathrm{GIC},i} = g_i V_i = g_i e_i^T \mathbf{V} = g_i e_i^T \mathbf{G}^{-1} \mathbf{I} \tag{4.13}$$

Now, the percentage variation of GIC in terms of the percentage variation of grounding resistance is expressed as follows:

$$\frac{\frac{\Delta I_{\mathrm{GIC},i}}{I_{\mathrm{GIC},i}}}{\frac{\Delta R_i}{R_i}} = \frac{g_i^2 \mathbf{R}_{ii} - g_i + g_i \tilde{g}_i \mathbf{R}_{ii} - \tilde{g}_i}{g_i + \mathbf{R}_{ii} g_i \tilde{g}_i} \tag{4.14}$$

In this equation, the driving point resistance R_{ii} is the element at the i-th row, i-th column of resistance matrix R. As stated in Section 4.1, matrix $\mathbf{G}$ is usually a sparse matrix so $\mathbf{R}$ can be computed efficiently using the sparse vector method [15].

From Eq. (4.14), the change of the GIC due to the change in its assumed local substation resistance can be calculated precisely. Taking the limit of Eq. (4.14) as the variation goes to 0 gives the desired sensitivity, which is the rate of change of GICs with respect to the variation of the assumed resistances.

$$S_{ii} = \lim_{\tilde{g}_{ii}\to 0} \frac{\frac{\Delta I_{\mathrm{GIC},i}}{I_{\mathrm{GIC},i}}}{\frac{\Delta R_i}{R_i}} = g_i \mathbf{R}_{ii} - 1 = \frac{\mathbf{R}_{ii}}{R_i} - 1 \tag{4.15}$$

Using Eq. (4.9), $\mathbf{R}_{ii}$ can be replaced by R_i and $R_{\mathrm{TH},i}$ and Eq. (4.15) can be rewritten as

$$S_{ii} = \frac{-1}{R_i + R_{\mathrm{TH},i}} \tag{4.16}$$

This equation is exactly the same as the GIC sensitivity to local substation grounding resistance derived in method 1.

4.2.2 Sensitivity of GICs to neighboring resistances

Next, the sensitivity of GIC at substation i to the variation of substation j grounding resistance, with $j \neq i$, is considered. This variation has an effect on the admittance matrix $\mathbf{G}$.

$$\mathbf{G}' = \mathbf{G} + \tilde{g}_j e_j e_j^T \tag{4.17}$$

where $\tilde{g}_j$ is the variation of the grounding conductance at substation j. Reemploying the matrix inversion lemma for this case, the inverse of matrix $\mathbf{G}'$ is given as

$$\mathbf{G}'^{-1} = \mathbf{G}^{-1} - \mathbf{G}^{-1} e_j (\tilde{g}_j^{-1} + e_j^T \mathbf{G}^{-1} e_j)^{-1} e_j^T \mathbf{G}^{-1} \tag{4.18}$$

Then, following the same procedure as in the derivation of local resistance in the previous section, the sensitivity of GICs at substation i to grounding resistance of substation j can be formulated as follows:

$$\frac{\frac{\Delta I_{\mathrm{GIC},i}}{I_{\mathrm{GIC},i}}}{\frac{\Delta R_j}{R_j}} = \frac{k g_j + k \tilde{g}_j}{1 + \mathbf{R}_{jj} \tilde{g}_j} \tag{4.19}$$

In this equation, $\mathbf{R}_{jj}$ is the element at row j, column j of resistance matrix $\mathbf{R}$, and k is a scalar number given by

$$k = \mathbf{R}_{ij} \frac{e_j^T \mathbf{G}^{-1} \mathbf{I}}{e_i^T \mathbf{G}^{-1} \mathbf{I}} = \mathbf{R}_{ij} \frac{V_j}{V_i} \tag{4.20}$$

where $\mathbf{R}_{ij}$ is the element at row j, column i of resistance matrix R, V_i and

V_j are neutral DC voltages of substations i and j. Similar to Eq. (4.14), Eq (4.19) is capable of providing the exact change of the GIC being studied given the change of the resistance. Taking the limit of Eq. (4.19) as the variation $\tilde{g}_j$ goes to 0 provides the rate of change of GICs at substation i with respect to the variation of the assumed resistances at substation j. In contrast to the local sensitivity, which is always negative, this sensitivity can be positive or negative depending on the signs of V_i and V_j. If the sensitivity is positive, an increase in the assumed grounding resistance leads to an increase in GIC and vice versa.

$$S_{ij} = \lim_{\tilde{g}_j \to 0} \frac{\frac{\Delta I_{\mathrm{GIC},i}}{I_{\mathrm{GIC},i}}}{\frac{\Delta R_j}{R_j}} = g_j \mathbf{R}_{ij} \frac{V_j}{V_i} = \frac{\mathbf{R}_{ij}}{R_j} \frac{V_j}{V_i} \tag{4.21}$$

As defined above, $\mathbf{R}_{ii}$ and $\mathbf{R}_{ij}$ are elements of matrix $\mathbf{G}^{-1}$. In a large system, $\mathbf{G}$ is usually sparse because each bus is only connected to a few other buses through the transmission lines. Hence the direct computation of $\mathbf{G}^{-1}$ will be redundant. As a result, the sparse vector method [15] is employed to obtain values of desired elements of matrix $\mathbf{G}^{-1}$. The idea is that all the sensitivities of GICs at substation i are in the column i-th of matrix $\mathbf{G}^{-1}$. Hence obtaining some particular sensitivity values of $I_{\mathrm{GIC},i}$ is equivalent to calculating some particular elements of the i-th column of $\mathbf{G}^{-1}$. In Equation (4.23), the i-th column of $\mathbf{G}^{-1}$ is denoted as x, and the i-th column of unit matrix $\mathbf{I}$ is denoted as b. Hence b is a vector in which all elements are 0 except the one at the i-th row. Using factorization, Eq. (4.24) can be rewritten as the combination of Eqs. (4.27) and (4.28). To solve for x, a forward substitution is first needed for $Ly = b$. Then a backward substitution for $Ux = y$ is carried out. Fortunately, because 1) b is a sparse vector and 2) only few elements of x are needed, fast forward (FF) and fast backward (FB) substitution techniques can be applied to solve these two equations. To use these techniques, factorization paths are needed for both L and U; each path is executed in forward order for FF and backward order for FB.

$$\mathbf{G}\mathbf{G}^{-1} = \mathbf{I} \tag{4.22}$$

$$\mathbf{G}(\mathbf{G}^{-1})_i = e_i \tag{4.23}$$

$$\mathbf{Gx} = \mathbf{b} \tag{4.24}$$

$$\mathbf{G} = \mathbf{LU} \tag{4.25}$$

$$\mathbf{LUx} = \mathbf{b} \tag{4.26}$$

$$\mathbf{Ly} = \mathbf{b} \tag{4.27}$$

$$\mathbf{Ux} = \mathbf{y} \tag{4.28}$$

CHAPTER 5

CASE STUDIES

5.1 EPRI 20-bus

Both algorithms from methods 1 and 2 are first demonstrated using the 20-bus test system from [19]. The one-line diagram of the system is shown in Figure 5.1. The arrows represent the flow of the GICs for the 1 V/km eastward field, while the size of an arrow is proportional to the magnitude of the GIC on each of the lines. The locations of the eight substations in the case are labeled in the figure. The algorithms are applied to the two GMD scenarios considered in [19], namely, a uniform 1 V/km eastward field and a uniform 1 V/km northward field.

For convenience, the assumed substation grounding resistance values and the calculated GIC flows for the two scenarios (from Tables I and VII of [19]) are given in Table 5.1. Notice that Substation 1 is modeled with a GIC blocking device so its grounding resistance is assumed to be infinite. Substation 7 models a series capacitor location that has no connection to ground.

Using the approach from Section 4.1 (method 1), the values for the 20-

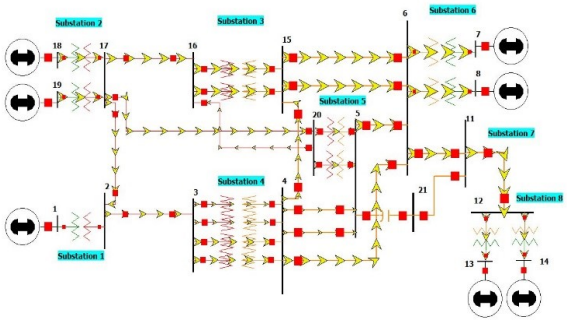

Figure 5.1: 20-bus GIC test system one-line showing 1 V/km eastward values

Table 5.1: 20-bus substation resistances and GIC flows

	Grounding resistance (Ω)	Eastward field GIC (A)	Northward field GIC (A)
Sub. 1	0.2 (but blocked)	0.00	0.00
Sub. 2	0.2	-189.29	115.63
Sub. 3	0.2	-109.49	139.85
Sub. 4	1.0	-124.58	19.98
Sub. 5	0.1	-65.46	-279.09
Sub. 6	0.1	354.52	-57.29
Sub. 7	No ground path	0.00	0.00
Sub. 8	0.1	134.30	60.9

Table 5.2: 20-bus substation equivalent values

	Driving point resistance (Ω)	R_{TH} (Ω)	$\Re$	V_{TH} eastward (V)	V_{TH} northward (V)
Sub. 2	0.158	0.750	0.210	-179.88	109.90
Sub. 3	0.115	0.272	0.424	-51.61	65.95
Sub. 4	0.198	0.246	0.802	-155.28	24.90
Sub. 5	0.076	0.321	0.239	-27.53	-117.41
Sub. 6	0.075	0.302	0.249	142.50	-23.02
Sub. 8	0.093	1.365	0.068	196.69	89.20

bus system are given in Table 5.1 (since grounding resistance plays no role for Substations 1 and 7, they are omitted from the table). Noted that the sensitivity of GIC to its local grounding resistance is independent of the GMD scenario, and depends only upon R_i and $R_{\mathrm{TH},i}$ (see Eq. 4.4); hence the values of $\Re$ in Table 5.2 are the same in two different scenarios here. The relatively low $\Re$ values for all the substations except 3 and 4 indicate that the substation GICs are not particularly dependent on the assumed substation resistance. In contrast, the GIC at Substation 4 is highly dependent on its grounding resistance value.

For example, if the Substation 4 grounding resistance value is assumed to decrease by 50% (from 1.0 to 0.5Ω), the new GIC for an eastward field would change from -124.6 A to -208.1 A (the magnitude increases by 67.01%). In contrast, at the less sensitive Substation 2, if its grounding resistance was also

Table 5.3: 20-bus system's sensitivity values for a uniform eastward field

	$I_{\mathrm{GIC},2}$	$I_{\mathrm{GIC},3}$	$I_{\mathrm{GIC},4}$	$I_{\mathrm{GIC},5}$	$I_{\mathrm{GIC},6}$	$I_{\mathrm{GIC},8}$
R_2	-0.210	0.121	0.028	0.250	-0.017	-0.004
R_3	0.040	-0.424	0.031	0.226	-0.052	-0.012
R_4	0.061	0.203	-0.802	0.691	-0.054	-0.013
R_5	0.015	0.040	0.019	-0.238	-0.015	-0.004
R_6	-0.030	-0.272	-0.044	-0.449	-0.249	0.133
R_8	-0.001	-0.009	-0.002	-0.015	0.019	-0.068

Table 5.4: 20-bus system's sensitivity values for a uniform northward field

	$I_{\mathrm{GIC},2}$	$I_{\mathrm{GIC},3}$	$I_{\mathrm{GIC},4}$	$I_{\mathrm{GIC},5}$	$I_{\mathrm{GIC},6}$	$I_{\mathrm{GIC},8}$
R_2	-0.210	0.058	0.107	-0.036	-0.066	0.006
R_3	0.085	-0.424	0.249	-0.068	-0.410	0.035
R_4	0.016	0.025	-0.802	-0.026	-0.054	0.005
R_5	-0.104	-0.135	-0.507	-0.238	0.404	-0.035
R_6	-0.008	-0.034	-0.044	0.017	-0.249	-0.047
R_8	0.001	0.003	0.004	-0.002	-0.053	-0.068

reduced by 50% (from 0.2 to 0.1 Ω), the Substation 2 GIC for the eastward field would only change from -189.3 to -211.6 A (the magnitude increases by 11.78%). The above sensitivity analysis confirms that the magnitude $\Re$ is indeed a sensitivity indicator.

Using the algorithm in method 2, the sensitivities of GICs to neighboring substation grounding resistances for the 1 V/km eastward field scenario are given in Table 5.3, and those for the 1 V/km northward field scenario are given in Table 5.4. Substation 1 and Substation 7 are also omitted in those tables. As mentioned above, the sensitivity to local grounding resistance does not depend on GMD scenarios. In contrast, the sensitivity to neighboring grounding resistances changes with the magnitude and direction of the solar storm. It means for different GMD scenarios, the sensitivities of a particular GIC to other substation resistances can be greatly different and need to be recomputed for each course of events. This can be proved by comparing the sensitivity values in Table 5.3 and Table 5.4.

From both tables, it is apparent that the absolute value of the sensitivity of a GIC to the local resistance is usually greater than those of the sensitivities to neighboring substation grounding resistances. However, there are still some cases in which the results are opposite. For convenience, the sensitivity

of the GIC at substation i with respect to the grounding resistance of substation j is denoted as S_{ij}. In Table 5.3, S_{55}, which is the sensitivity of GIC at Substation 5 to its grounding resistance, is -0.238 but its sensitivities to Substation 4 and Substation 6 resistances are 0.691 and -0.449, respectively. The fact that the absolute values of S_{54} and S_{56} are greater than that of S_{55} means if the GIC value at Substation 5 is important then accurate values of the resistances of Substation 4 and 6 are needed more than that of Substation 5. This situation also happens for GIC at Substation 6 in Table 5.4 where the absolute value of S_{66} (-0.249) is smaller than those of S_{63} (-0.410) and S_{65} (0.404). In addition, in the case of GIC at Substation 4, even though the absolute value of S_{45} (-0.507) is not greater than that of S_{44} (-0.802), it is still significant; hence the accuracy of the grounding resistance of Substation 5 should still be considered in calculating GIC_4. This example shows that the calculation of the sensitivity to neighboring substation grounding resistance is not redundant but necessary.

Even though the 20-bus test case only has few substations, there are still two remarks prompted by Tables 5.3 and 5.4. First, the absolute value of the sensitivity of a GIC to the local resistance is frequently greater than most of the sensitivities to other substation grounding resistances. This result implies that, regularly, the accurate value of the local resistance has the largest share in the calculation of GIC. Secondly, most of the external sensitivity values in both tables are trivial (smaller than 0.1) and the non-trivial ones are only a handful. In addition, all of them are sensitivity of GIC to grounding resistances of substations that are directly connected or two hops away from the substation being studied. This observation reveals that only grounding resistances from nearby substations contribute significantly to the sensitivity of GIC; this aspect will be examined further in the following section.

5.2 150-bus synthetic system

In studies of geomagnetic disturbances, there are only few realistic test cases that are not restricted by data confidentiality. Since they are large, they mostly contain critical infrastructure information that is restricted to use for public validation of GMD analysis. Birchfield et al. [20] provide a method to generate a completely synthetic transmission system. It utilizes public

energy and census data to form the basis for generation, load, and geographic substation placement. The approach is to build a large synthetic power system which matches statistical characteristics of the actual transmission line, like the Eastern Interconnect (EI) in North America.

Using the method presented, [20] introduces a 150-bus synthetic network created based on the State of Tennessee's power system, which is part of EI. This test case that will be used for GIC sensitivity analysis in this section. The power system of Tennessee contains 98 substations with a geographic footprint covering approximately 35^oN to 36.5^oN latitude and 90^oW to 82^oW longitude; the wide geographic area makes it better for GIC analysis. 500 kV and 230 kV were chosen as the nominal voltage levels because of their low resistance and long transmission distance. Since the most of the substation grounding resistances in this system are not known, their values are assigned based on the assumed size of the substations which includes the nominal voltage level and the number of buses in them. The larger, higher voltage substations have lower resistance values.

For this case study, consider a uniform 3 V/km eastward electric field applied on the synthetic system being studied. The purpose of applying a uniform electric field is not to imply such a field would represent a realistic GMD storm scenario; rather it is used solely to generate example GICs. Note that in this system, all 230 kV substations have only one voltage level so they do not connect to any transformer and therefore do not have GIC value. Hence, only 500 kV substations are examined for GIC sensitivity analysis in this case. In Figure 5.2, all substations are presented as boxes with the orange one being 500 kV and the blue one 230 kV. Among 98 substations in the network, there are twenty-seven 500 kV substations with a GIC magnitude of 3.96 A to 461.6 A. Table 5.5 presents fifteen substations with the highest GICs, and Figure 5.2 shows them marked on the one-line diagram of the 150-bus system. Publishing these data in the case of an actual grid like EI would violate data confidentiality; using a synthetic system helps avoid that issue while still providing a realistic case study for GIC analysis.

According to Table 5.5, the sensitivities to local grounding resistance of all fifteen substations are non-trivial (larger than 0.1), indicating that the assumed resistance dominates in determining the GIC for a particular substation. Moreover, more than half of them (8 out of 15) have sensitivity at or above 0.4. To illustrate, consider Substation 78 which has an assumed

Table 5.5: 150-bus system's 15 substations with the largest GICs and their local sensitivity values for a 3V/km eastward field

Sub #	Assumed R(Ω)	GIC(A)	Sensitivity
44	0.18	461.6	-0.356
93	0.11	-460.45	-0.429
78	0.18	-419.61	-0.461
91	0.12	350.13	-0.366
42	0.18	303.7	-0.427
95	0.11	-273.18	-0.41
70	0.18	-214.76	-0.44
94	0.12	-206.53	-0.45
96	0.15	158.44	-0.227
85	0.18	-131.53	-0.402
97	0.11	128.8	-0.463
26	0.18	-124.12	-0.383
89	0.18	121.1	-0.361
21	0.18	117.92	-0.359
92	0.12	95.22	-0.369

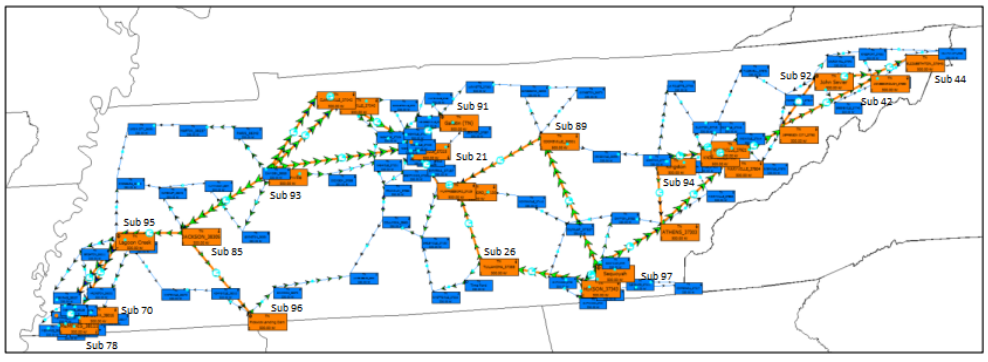

Figure 5.2: One-line diagram of 150-bus GMD test case with marks on 15 substations with highest GICs

Table 5.6: 150-bus system non-trivial external sensitivity values of 15 substations

Substation of GIC	Substation of resistance	Sensitivity	# of hops
42	44	0.209	1
85	93	0.173	1
85	95	0.147	1
95	70	0.134	1
95	78	0.286	1
70	78	0.359	1
70	95	0.133	1
21	91	0.358	1
21	93	-0.183	1
92	42	0.489	1
92	44	0.546	2

grounding resistance of 0.18 Ω and sensitivity of -0.461; its GIC magnitude of 419.61 A in this scenario indicates that it is highly susceptible to GIC on its GSUs. If the assumed grounding resistance is increased from 0.18 to 0.5 Ω, then the magnitude would drop by half to 229.86 A. On the other hand, if the limit of GIC value the substation can handle is 500 A and the actual value of its grounding resistance is 0.1 Ω, the imprecise calculation of GIC may lead to damage to transformers in the substation due to lack of a protection scheme.

Besides the local grounding resistance, GICs in these substations are also dependent on the assumed resistances of neighboring substations. Similar to the 20-bus system case, most of the external sensitivities in this case are very small and can be ignored. However, there are still a handful of values that are non-trivial and are presented in Table 5.6. The result reaffirms that the influence of external grounding resistances on the calculation of GIC at a particular substation cannot be overlooked. In addition, the last column in Table 5.6 shows the relative distance between the GIC's substation and the external resistance's substation. If the value is 1 then the two substations are directly connected to each other. If it is 2 then they are connected through a substation in the middle. The values in this column indicate that a GIC is only affected by the grounding resistances of nearby substations, which is also acknowledged in the end of Section 5.1.

CHAPTER 6

CONCLUSION

This thesis has addressed the issue of the sensitivity of the GICs to the assumed (either local or neighboring) substation grounding resistance in the system, providing an algorithm suitable for large system use to quantify this sensitivity. The conclusion of the thesis is that the GICs can indeed be quite dependent on these values, with example results provided for the 20-bus GIC test system and the 150-bus synthetic system.

Another contribution of this thesis is a methodology for identifying the substations that need accurate grounding resistance values: those substations that have high GICs and high sensitivity values. Ideally, utility engineers would have easy access to data sets that provide accurate values for all substations in a network. However, this can be difficult in practice as was discussed in Section 2.3. The methodology introduced in this thesis can help them focus on the locations in which accurate information is most needed.

REFERENCES

[1] "Getting down to earth: A practical guide to ground resistance testing," pp. 1–41, 2010.

[2] T. Dodrill, "NASA spots fast moving solar flare." [Online]. Available: http://www.offthegridnews.com/grid-threats/nasa-spots-fast-moving-solar-flare/

[3] "Power industry protection from solar storms." [Online]. Available: http://solar.spacew.com/gic/index.html

[4] "IEEE guide for measuring earth resistivity, ground impedance, and earth surface potentials of a grounding system," *IEEE Std 81-2012 (Revision of IEEE Std 81-1983)*, pp. 1–86, Dec 2012.

[5] T. Hutchins, "Geomagnetically induced currents and their effect on power systems," Ph.D. dissertation, University of Illinois at Urbana-Champaign, 2012.

[6] V. D. Albertson, J. M. Thorson, R. E. Clayton, and S. C. Tripathy, "Solar-induced-currents in power systems: cause and effects," *IEEE Transactions on Power Apparatus and Systems*, no. 2, pp. 471–477, 1973.

[7] North American Electric Reliability Corporation, "2012 special reliability assessment: Interim report: Effects of geomagnetic disturbances on the bulk power system," February, 2012.

[8] V. Albertson, J. Kappenman, N. Mohan, and G. Skarbakka, "Load-flow studies in the presence of geomagnetically-induced currents," *IEEE Transactions on Power Apparatus and Systems*, no. 2, pp. 594–607, 1981.

[9] J. Kappenman, *Geomagnetic Storms and Their Impacts on the US Power Grid*. Metatech Corp., 2010.

[10] T. J. Overbye, T. R. Hutchins, K. Shetye, J. Weber, and S. Dahman, "Integration of geomagnetic disturbance modeling into the power flow: A methodology for large-scale system studies," in *North American Power Symposium (NAPS), 2012*. IEEE, 2012, pp. 1–7.

[11] T. J. Overbye, K. S. Shetye, Y. Z. Hughes, and J. D. Weber, "Preliminary consideration of voltage stability impacts of geomagnetically induced currents," in *2013 IEEE Power & Energy Society General Meeting*. IEEE, 2013, pp. 1–5.

[12] North American Electric Reliability Corporation and the United States Department of Energy, "High-impact, low-frequency event risk to the North American bulk power system," June, 2010.

[13] E. B. Curdts, "Some of the fundamental aspects of ground resistance measurements," *Transactions of the American Institute of Electrical Engineers, Part I: Communication and Electronics*, vol. 77, no. 5, pp. 760–767, Nov 1958.

[14] R. Pirjola, "Study of effects of changes of earthing resistances on geomagnetically induced currents in an electric power transmission system," *Radio Science*, vol. 43, no. 1, 2008.

[15] W. Tinney, V. Brandwajn, and S. Chan, "Sparse vector methods," *IEEE Transactions on Power Apparatus and Systems*, no. 2, pp. 295–301, 1985.

[16] V. D. Albertson and J. A. V. Baelen, "Electric and magnetic fields at the earth's surface due to auroral currents," *IEEE Transactions on Power Apparatus and Systems*, vol. PAS-89, no. 4, pp. 578–584, April 1970.

[17] D. Boteler and R. Pirjola, "The complex-image method for calculating the magnetic and electric fields produced at the surface of the earth by the auroral electrojet," *Geophysical Journal International*, vol. 132, no. 1, pp. 31–40, 1998.

[18] K. Zheng, D. Boteler, R. Pirjola, L. Liu, R. Becker, L. Marti, S. Boutilier, and S. Guillon, "Influence of system characteristics on the amplitudes of geomagnetically induced currents," submitted to *IEEE Trans on Power Delivery*, 2012.

[19] R. Horton, D. Boteler, T. J. Overbye, R. Pirjola, and R. C. Dugan, "A test case for the calculation of geomagnetically induced currents," *IEEE Transactions on Power Delivery*, vol. 27, no. 4, pp. 2368–2373, 2012.

[20] A. B. Birchfield, K. M. Gegner, T. Xu, K. S. Shetye, and T. J. Overbye, "Statistical considerations in the creation of realistic synthetic power grids for geomagnetic disturbance studies," *IEEE Transactions on Power Systems*, vol. PP, no. 99, pp. 1–1, 2016.